UNLV | UNIVERSITY LIBRARIES

Transmutation Sciences Materials (TRP) | Transmutation Research Program Projects

10-2-2003

# Modeling, Fabrication, and Optimization of Niobium Cavities: Phase III Quarterly Report

Robert A. Schill Jr.
*University of Nevada, Las Vegas*, robert.schill@unlv.edu

Mohamed Trabia
*University of Nevada, Las Vegas*, mbt@me.unlv.edu

Follow this and additional works at: https://digitalscholarship.unlv.edu/hrc_trp_sciences_materials

 Part of the Electrical and Computer Engineering Commons, Mechanical Engineering Commons, Metallurgy Commons, and the Nuclear Engineering Commons

## Repository Citation

Schill, R. A., Trabia, M. (2003). Modeling, Fabrication, and Optimization of Niobium Cavities: Phase III Quarterly Report. 1-32.
**Available at:** https://digitalscholarship.unlv.edu/hrc_trp_sciences_materials/10

This Report is protected by copyright and/or related rights. It has been brought to you by Digital Scholarship@UNLV with permission from the rights-holder(s). You are free to use this Report in any way that is permitted by the copyright and related rights legislation that applies to your use. For other uses you need to obtain permission from the rights-holder(s) directly, unless additional rights are indicated by a Creative Commons license in the record and/or on the work itself.

This Report has been accepted for inclusion in Transmutation Sciences Materials (TRP) by an authorized administrator of Digital Scholarship@UNLV. For more information, please contact digitalscholarship@unlv.edu.

# Modeling, Fabrication, and Optimization of Niobium Cavities –Phase III
# Quarterly Report

**Principal Investigators (PI):** Robert A. Schill, Jr.
Department of Electrical & Computer Engineering, UNLV
4505 Maryland Parkway, Las Vegas, NV 89154-4026
Phone: (702) 895-1526
Email: schill@ee.unlv.edu

Mohamed B. Trabia
Department of Mechanical Engineering, UNLV
4505 Maryland Parkway, Las Vegas, NV 89154-4027
Phone: (702) 895-0957
Email: mbt@me.unlv.edu

**Investigator:** William Culbreth
Department of Mechanical Engineering, UNLV
4505 Maryland Parkway, Las Vegas, NV 89154-4027
Phone: (702) 895-3426
Email: culbreti@nscee.edu

**Current Students:** S. Subramanian (Graduate Student)
Anoop George (Graduate Student)
Myong Holl (Undergraduate Student)

**Collaborators (DOE):** Dr. Tsuyoshi Tajima, Team Leader
Accelerator Physics & Engineering
LANSCE-1
Los Alamos National Laboratory
MS H817
Los Alamos, NM 87545
Phone: (505) 667-6559
Email: tajima@lanl.gov

**AAA Research Area**: Accelerators / Transmuter

**Abstract**

Niobium cavities are important parts of the integrated NC/SC high-power linacs. Over the years, researchers in several countries have tested various cavity shapes. They concluded that elliptically shaped cells are the most appropriate shape for superconducting cavities. The need for very clean surfaces lead to the use of a buffered chemical polishing produce for surface cleaning to get good performance of the cavities. The third phase concludes the experimental a fluid flow study and optimization study. The first quarter and second quarter of phase three also begins the experimental set-up of secondary emission studies from niobium in superconducting mode. This study is to be completed by the end of the third year.

**Introduction**

The nuclear industry provides a significant percentage of the world, including the United States, with electricity. Nuclear power plants produce thousands of tons of spent fuel. Some of this spent fuel can be radioactive for thousands of years. The US DOE is currently exploring the possibility of creating a permanent storage site at Yucca Mountain, Nevada for nuclear spent fuel. Accelerator Transmutation of Waste is one complementary approach to deal with spent nuclear fuel. In this approach, a particle accelerator produces protons that react with a heavy metal target to produce neutrons. These neutrons are used to transmute long-lived radioactive isotopes into shorter-lived isotopes that are easier to be handled. A major component of the system is a linear accelerator (linac) that can accelerate a 100-mA beam of protons up to 1 GeV [1]. Los Alamos National Laboratory (LANL) is an active participant in developing a superconducting rf (SCRF) high-current linear accelerator. SCRF has three major components: niobium cavities, power couplers, and cryomodules. This effort mainly deals with niobium cavities.

Niobium cavities have several advantages including small power dissipation compared to normal conducting copper cavities. These cavities are usually made of multiple elliptical cells. Refer to Figure 1. They are formed from sheet metal using various techniques such as deep drawing or spinning. The cells then are welded using electron-beams. Multi-cell units are usually tuned by stretching or squeezing them. Niobium cavities need very clean surfaces, which can be achieved by chemical polishing and high pressure rinsing with ultra-pure water.

Under operation very high electromagnetic fields are present in these cavities. Besides the intended acceleration of a particle beam, these fields can also accelerate electrons emitted from the niobium surfaces. An electron emitted from the surface of the cavity wall is guided and accelerated by these RF-fields until it impacts on the cavity surface again. This impact can lead to the generation of one or more secondary electrons that in turn act as primary electrons. In turn, these electrons may generate more electrons in a localized region. The number of secondary electrons is determined by the impact energy of the electron and by the secondary emission coefficient of the cavity material. If secondary electrons are created in phase with the RF-fields, and the impact is localized, a rapidly rising multiplication of electrons will occur. This localized resonant process is known as *multipacting* (multiple impacting). Consequently, RF power is absorbed. It becomes increasingly difficult to increase the RF energy in the cavity as the power supplied to the cavity is increased. The electron collisions with the structure walls lead to a temperature rise and eventually to a breakdown of the superconductivity. As a result, the $Q_0$ (quality factor) of the cavity is significantly reduced at the multipacting thresholds. In addition, structural damage of the surface can occur. A good cavity design should be able to eliminate, or at least minimize multipacting. The factors that affect multipacting include: shape, surface finish, and coating.

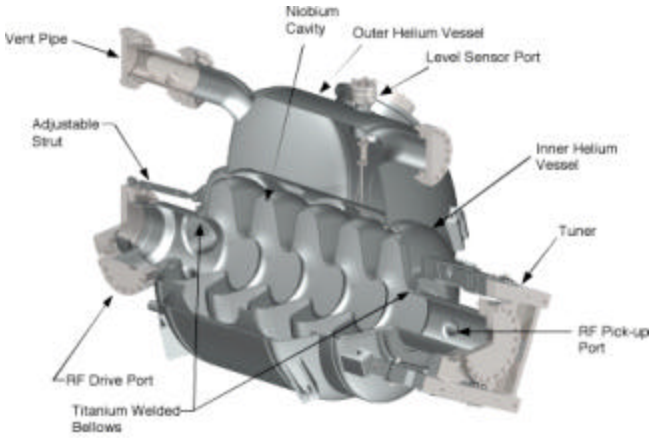


**Figure 1.** Schematic Diagram of Niobium Cavities (Executive Summary: Development and Performance of Medium-Beta Superconducting Cavities (LANL))

While models have been suggested for minimizing multipacting [2], a practical means of manufacturing the cavity walls to obtain optimal designs are still an issue. Attempting to improve the performance of multiple niobium cavities may be a daunting task because of the computational load associated with the evaluation of a particular design and the large number of variables and constraints involved. We propose approaching this task in a systematic way using principles of nonlinear programming. The consequence of this effort will allow the Superconducting RF Engineering Development and Demonstration group at LANL and the faculty at UNLV to target potential cavity cell configurations that improve upon existing designs.

**Summary of Achievements of Phase III:**

1. Multipacting Studies: A significant amount of time has been spent on evaluating possible multipacting scenarios using the research code provided to us by Field Precision. Running thousands of particle simulations on simple muffin cavity geometry has not resulted in actual evidence of multipacting. Impacting with multiple hits can always be found. Results do not appear to yield clear cut evidence of multipacting. One may deduce that multipacting might occur by examining the probability that a secondary electron is emitted from the surface of the material under test. In this case, one narrows in on those primary electrons exhibiting a large number of impacts. A primary electron yielding ten impacts may have a high enough probability of generating a couple of secondary electrons. Particles exhibiting a large numbers of impacts are sought. Once identified, their particle orbits are then examined to determine if they exhibit some periodic trajectory. This periodic motion is a sign of multipacting. Many of the particles exhibiting large numbers of orbits do exhibit this periodic motion but the probability of secondary emission is low on an impact. Further the particle orbit is usually terminated because the emitted charge does not have enough kinetic energy to overcome the binding energy of the surface of the niobium under test. The major difficulty that arises with the application of the code is repeatability. The random number generator internal to the code used as an aid in characterizing the surface and bulk physics of the medium inhibits repeatability. Figure 2 shows two different runs. In each case, 10 identical particles are released with the exact same initial conditions. All ten particles in each figure follow the same trajectory to the wall. When the particles impact the wall, all ten trajectories change dramatically. The impact point is where all of the colored trajectory lines emanate from in the figures. Thousands of particle runs have been conducted in the muffin tin cavity and the beta-64 cavity.

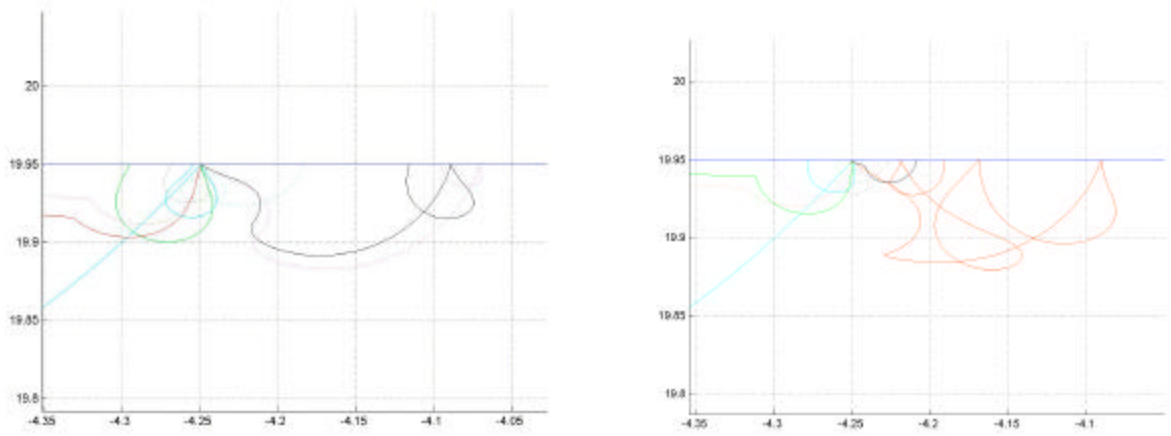


**Figure 2.** Typical particle trajectory with multiple impacts. Ten particles were release with the exact same initial conditions and the exact same boundary conditions. In all cases, the cumulative multipacting factor was less than 1. One indication of multipacting occurs when the cumulative multipacting factor exceeds one for an electron exhibiting periodic impacts over the duration of the program run. Notice that none of the orbit trajectories are the same.

2. Experimental Set-up for the SEE from a Niobium Test Piece. Near the end of phase II, an existing vacuum chamber was modified for SEE studies. Through various donations, a cryogenic

pump with controller was obtained. An electron gun, heat tape, and a residual gas analyzer (RGA) were received. To save about $55,000 or more, the insides of an old cryogenic pump has been converted to a cryostat. The "cryostat" was tested by the manufacturer and will reach superconducting temperatures for niobium (~8 $^{o}$K). Sensor studies were conducted. These activities were reported in past quarterly reports and final reports during phase II. Funding was obtained through phase III of the research to set-up and run secondary electron emission studies of niobium in the superconducting state.

During the first quarter of phase III, sensor studies were completed. With the aid of a grid, field and geometry requirements for a position sensitive MCP/RAE electron sensor, electron gun specifications, sample size and cryostat geometry, optimal locations and potentials were obtained to detect single secondary electrons emitted from a niobium sample with various energies and trajectories. Figure 3 illustrates the current geometry of the niobium piece under test. For practical reasons, the geometry may be modified by placing a number of known bevels over the hemispherical surface. This will aid in eliminating alignment issues. Figures 4 and 5 show typical single particle trajectories in the designed system for worst case scenarios. For example, the primary electron beam diameter to be used in experiment is on the order of 25 μm. Figures 4a and 5a have employed beam diameters of 1 mm. Therefore, those outer particles diverging significantly from the sample surface are not of interest except when it comes to alignment issues. For the most part, increasing the beam energy by a factor of five significantly decreases the beam divergence. Figures 4b,c and 5b,c also yield worst case scenarios regarding initial particle energy and trajectory. With a proper grid potential, all secondary electrons can be collected. Table 1 provides the parameters associated with the experimental setup of Figs. 4 and 5. Upon completion of the study, Roent Dek's MCP/RAE electron position detector and power system was ordered. The sensor has a spatial resolution between 50 to 800 μm and can detect single energetic electrons. It is anticipated that the detector will arrive late in the second quarter or early third quarter. The dimension of the grid was determined and ordered from Dexmet Corporation. Although an electron gun was ordered, an unforeseen natural hurricane disaster out east has delayed the design and building of the gun. By the end of the second or early in the third quarter it is anticipated that the electron gun will be installed on the vacuum chamber. Sensors in the electron gun will not be able to detect the currents and charge required for the position detector to work properly. As a result, a Faraday cup will be incorporated in the design to measure the electron beam charge and current averaged over a period of time. An electrometer will be used to make this measurement. The Faraday cup will be inserted in front of the beam for calibration purposes prior to performing the experiment. The experimental environment will be in high vacuum with test piece in its cryogenic state. The cup will be removed from the experimental region *in situ* by means of a manipulator arm internal to the chamber. The manipulator arm has a number of functions. Refer to Figs. 6 and 7. It will be used to initially position the sample under test for alignment with the beam. It will also provide a means for *in situ* cleaning. Literature has indicated that carbons or hydrocarbons are hard to eliminate from the cold surfaces. A gas containing a large inert molecule or atom such as argon or argon combined with a chemically reactive gas, in particular, helium will be puffed between the sample and a high voltage electrode. The Ar is used to perform the sputtering process due to its large atomic mass where as the $H_2$ is used to chemically react with the carbon to form methane which then can be pumped out of the system. The manipulator arm supports the electrode and gas tube. Literature has also indicated that under "cold" (not necessarily cryogenic) conditions, water sorbed on the surface of niobium significantly affects the secondary electron emission properties. In order to minimize water on the surface of the piece under test, a 15 W quartz lamp with mirror arrangement will be used to heat the

surface of the niobium. This will be used as a last step in the cleaning process before conducting the experimental. A small wattage lamp is required to prevent large temperature gradients at the surface of the cryostat. Further, a GaIn alloy is to be used to adhere the sample under test to the surface of the cryostat. At room temperature, the alloy is in liquid form. Slightly below $25^{o}$ C, it becomes a solid. GaIn has good conduction properties needed to maintain an $8^{o}$ K environment in the niobium sample. The alloy was recently ordered from Indium Corporation of America. Vertical alignment of the system under vacuum pressure is of importance for the gun, detector, and sample system to appropriately operate using the predicted voltages. At this time, a stiff bellows will be attached to the cryostat to offer some vertical alignment adjustment. Refer to Fig. 7.

**Table 1.** Typical design parameters and initial particle trajectory conditions.

| **Parameters** | **Figure 4a,b,c** | **Figure 5a,b,c** |
|---|---|---|
| | | |
| Vertical distance between gun and position detector | 30 mm | 30 mm |
| Vertical distance between position detector and grid | 3 mm | 3mm |
| Vertical distance between grid and upper most position of piece under test | 22 mm | 22 mm |
| Overall thickness of niobium test piece simulated ***(actual thickness is 1 cm max.)*** | 0.5 cm | 0.5 cm |
| Cylindrical Radius of niobium test piece | 5 mm | 5 mm |
| Radius of particle position detector | 47 mm | 47 mm |
| Radius of grid | 63 mm | 63 mm |
| Grid mesh size (opening) | 1.2 mm | 1.2 mm |
| Grid potential | 0 V | 1 kV |
| Potential of electron gun casing | 0 V | 0 V |
| Potential of particle detector | 4 kV | 4 kV |
| Potential of niobium test piece | 0 V | 0 V |
| Initial energy of primary beam ***(worst case scenario for a lower limit)*** | 50 eV (a) | 50 eV (a) |
| Final energy of primary beam upon impact | 46 eV | 49 eV |
| Trajectory of primary beam relative to normal of niobium surface | 0 deg. | 64 deg. |
| Primary Beam Diameter at Gun [Target] ***NOTE: a 20 mm beam diameter is planned to be used; here we are looking at worst case scenarios*** | 1 mm [10 mm] | 1 mm [20 mm] |
| Initial secondary electron launch angles relative to the normal of the niobium surface (40 trajectories) ***(worst case scenarios presented at range extremes)*** | Range $-90^{o}$ to $90^{o}$ in $4.5^{o}$ increments | Range $-90^{o}$ to $90^{o}$ in $4.5^{o}$ increments |
| Initial secondary electron energies ***(Typical range)*** | 1 eV (b); 20 eV (c) | 1 eV (b); 20 eV (c) |
| Niobium test piece offset dimension from beam axis | 0 mm | 4.5 mm |

A secondary electron emission code is being sought in the community to aid this research study. Results obtained from experiment should be backed up by physics showing relevance to the measured data. It may be possible to obtain a simple secondary electron emission code from Dr. Joy at ORNL.

Early in the second quarter, a scheme to position different portions of the surface of the niobium sample under the electron beam without the need to warm the cryostat and re-pump the system is being sought. This will save roughly eight to sixteen hours between each data point gained in the experiment. Besides logistics, space tolerances will be a challenge. The manipulator design should be completed and placed on order in the second quarter. In the second quarter, the vacuum system will be tested against leaks using the RGA and, if necessary, a differential pumping technique. During the second quarter, LANL will be requested to develop niobium samples needed for our experiment. A six-week waiting period is anticipated before samples will be sent to UNLV.

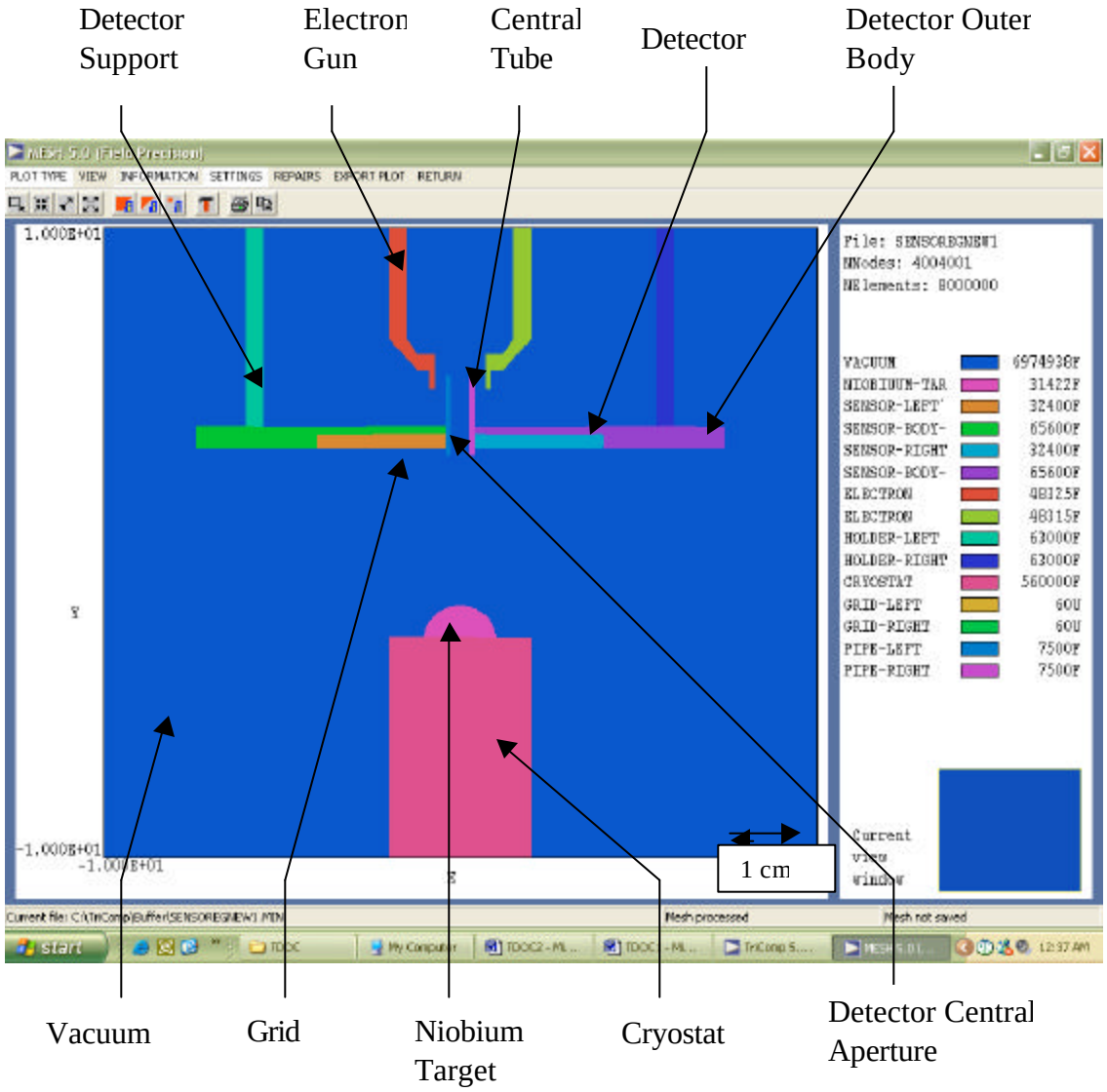


**Figure 3.** Simple geometry of niobium piece under test.

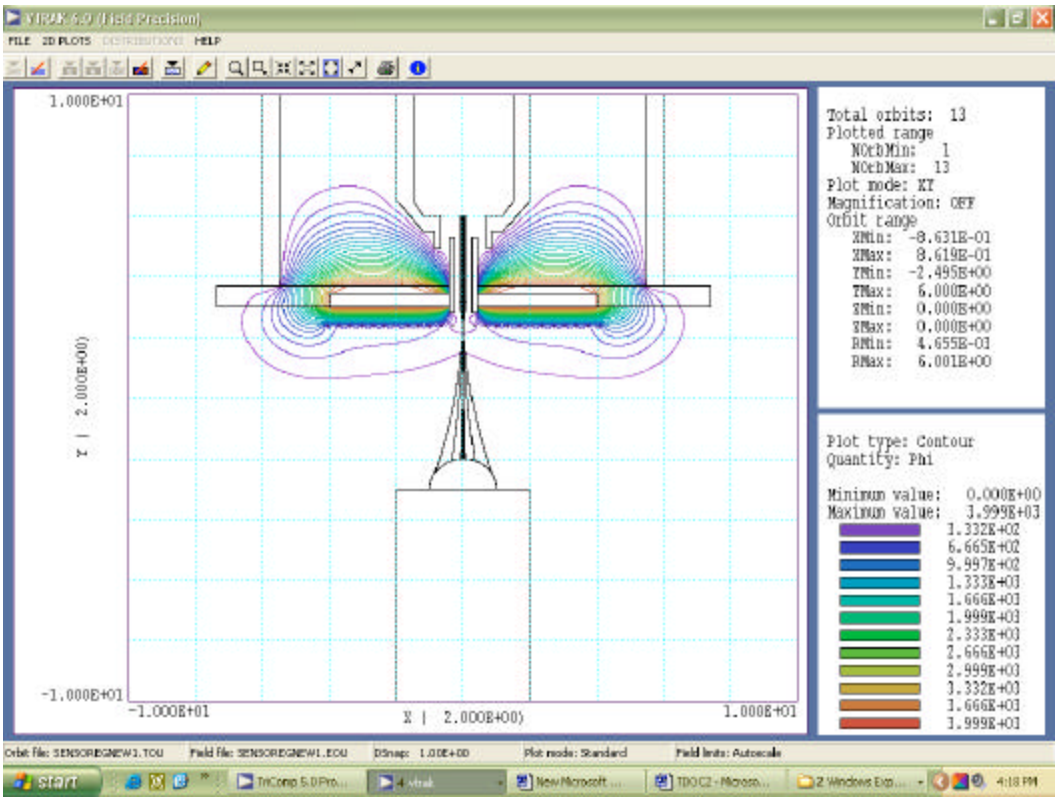
1.000E+01
Y | 2.000E+00
-1.000E+01
-1.000E+01
X | 2.000E+00
1.000E+01
Total orbits: 13
Plotted range
NOrbMin: 1
NOrbMax: 13
Plot mode: XY
Magnification: OFF
Orbit range
XMin: -8.631E-01
XMax: 8.619E-01
YMin: -2.495E+00
YMax: 6.000E+00
ZMin: 0.000E+00
ZMax: 0.000E+00
RMin: 4.655E-01
RMax: 6.001E+00
Plot type: Contour
Quantity: Phi
Minimum value: 0.000E+00
Maximum value: 3.999E+03
1.332E+02
6.665E+02
9.997E+02
1.333E+03
1.666E+03
1.999E+03
2.333E+03
2.666E+03
2.999E+03
3.332E+03
1.666E+03
1.999E+03

**(4a)**

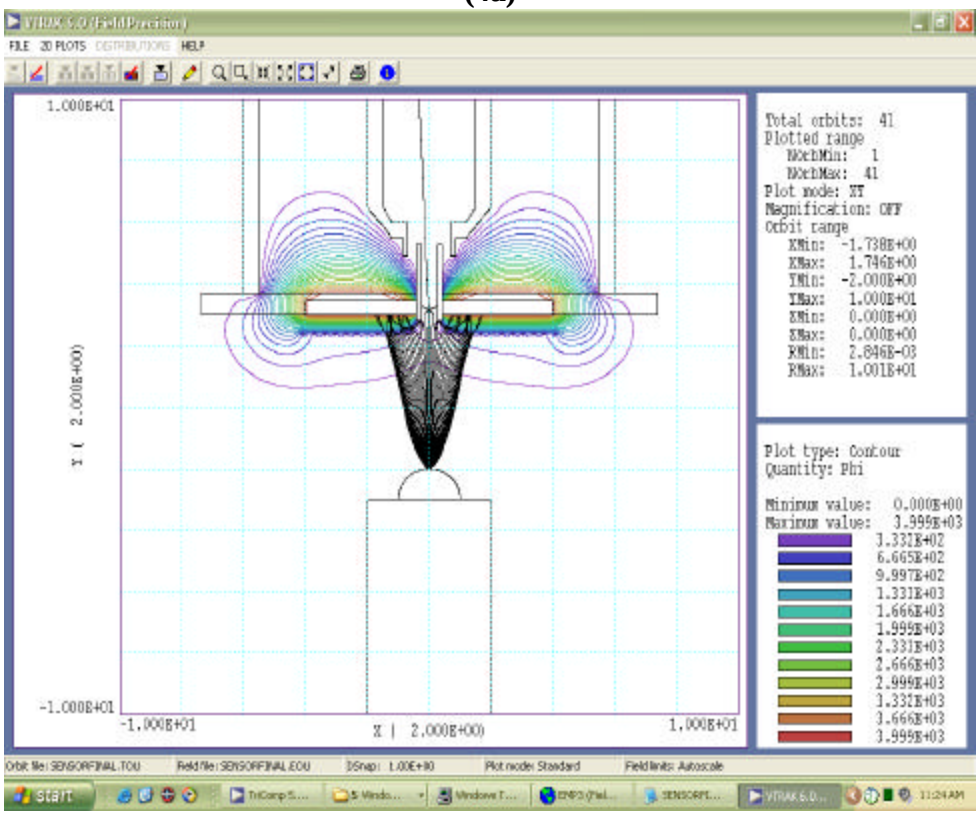
1.000E+01
Y | 2.000E+00
-1.000E+01
-1.000E+01
X | 2.000E+00
1.000E+01
Total orbits: 41
Plotted range
NOrbMin: 1
NOrbMax: 41
Plot mode: XY
Magnification: OFF
Orbit range
XMin: -1.738E+00
XMax: 1.746E+00
YMin: -2.000E+00
YMax: 1.000E+01
ZMin: 0.000E+00
ZMax: 0.000E+00
RMin: 2.846E-03
RMax: 1.001E+01
Plot type: Contour
Quantity: Phi
Minimum value: 0.000E+00
Maximum value: 3.995E+03
3.331E+02
6.665E+02
9.997E+02
1.331E+03
1.666E+03
1.999E+03
2.331E+03
2.666E+03
2.999E+03
1.331E+03
1.666E+03
1.999E+03

**(4b)**

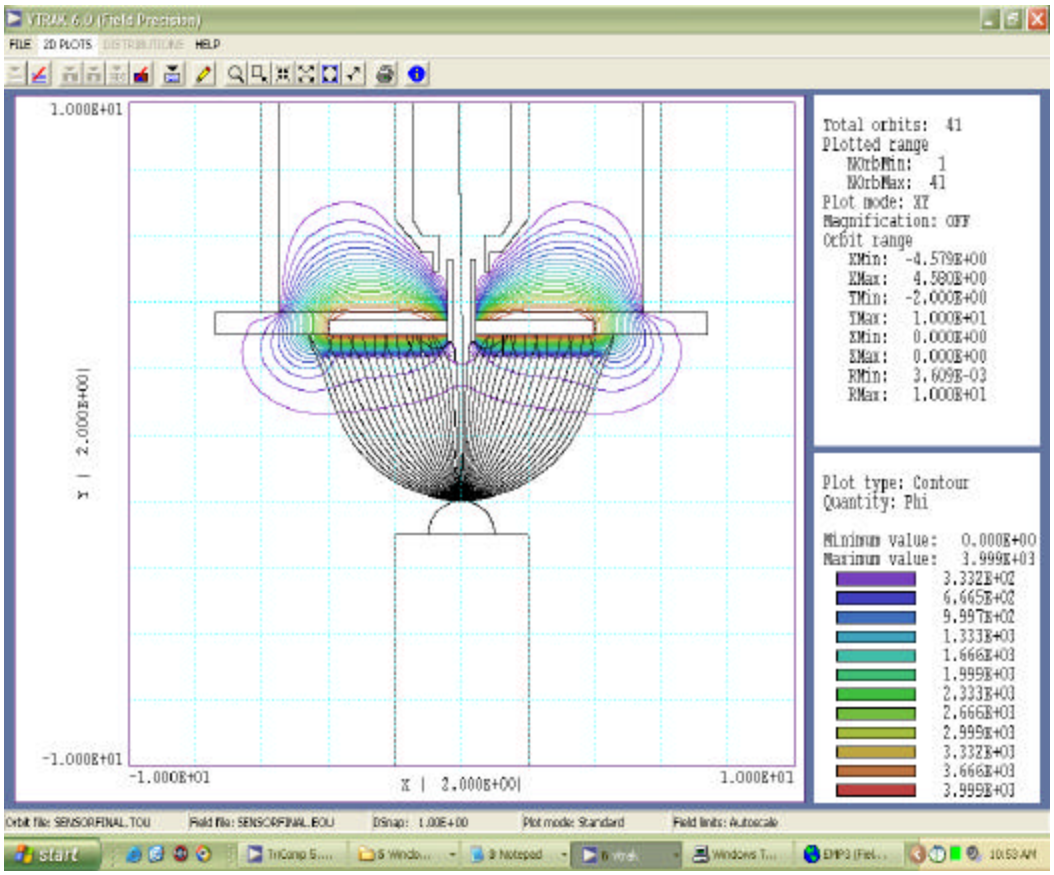


**(4c)**

**Figure 4.** Optimal system design where: (a) shows 50 eV primary particle trajectories, (b) illustrates secondary electron trajectories with 2 eV initial energies, and (c) with 20 eV initial energy trajectories. A grid is used to accelerate the captured secondary electron towards the particle position detector. The grid also aids in maintaining a somewhat field free condition between the grid and niobium test piece. A tube is required between the electron gun and the particle detector to shield the primary electron beam from stray electric field due to potential differences between the gun and electron detector. Note that the grid hole size is important to prevent stray fields to inadvertently influence either the primary electron beam or the secondary electron beam trajectory. Table 1 provides some of the design parameters and the initial particle parameters.

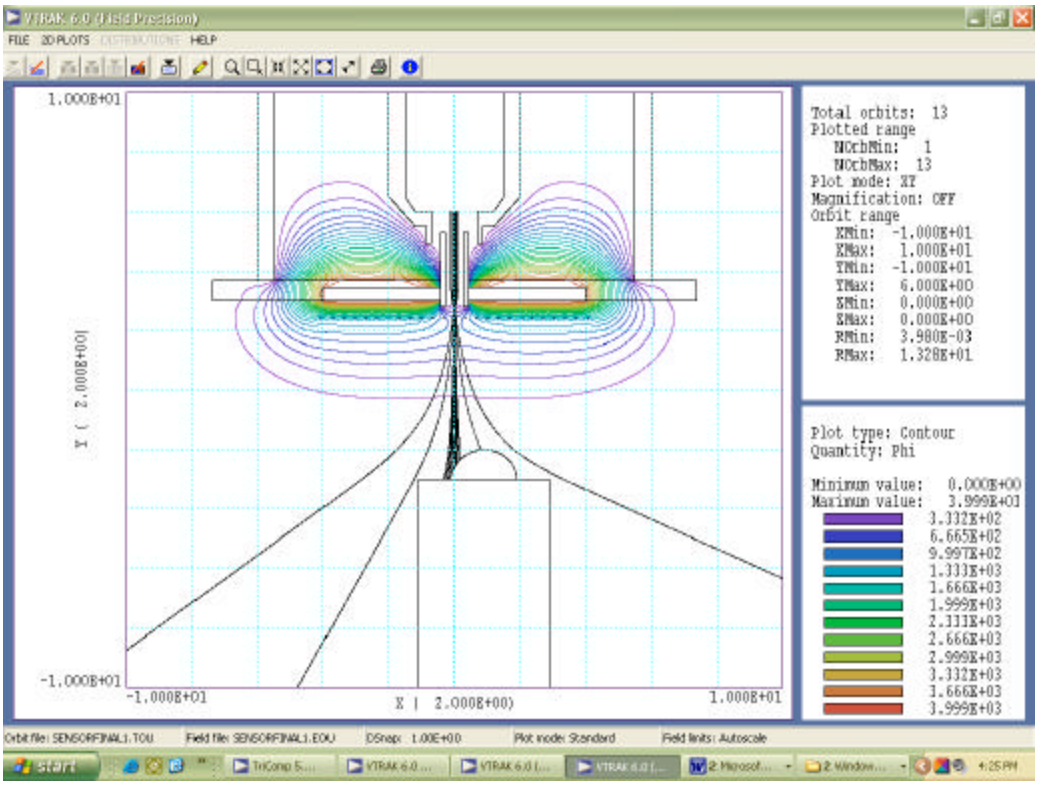
FILE 2D PLOTS HELP
1.000E+01
Y ( 2.000E+00)
-1.000E+01
-1.000E+01
X ( 2.000E+00)
1.000E+01
Total orbits: 13
Plotted range
NOrbMin: 1
NOrbMax: 13
Plot mode: XY
Magnification: OFF
Orbit range
XMin: -1.000E+01
XMax: 1.000E+01
YMin: -1.000E+01
YMax: 6.000E+00
SMin: 0.000E+00
SMax: 0.000E+00
RMin: 3.980E-03
RMax: 1.328E+01
Plot type: Contour
Quantity: Phi
Minimum value: 0.000E+00
Maximum value: 3.999E+03
3.332E+02
6.665E+02
9.997E+02
1.333E+03
1.666E+03
1.999E+03
2.111E+03
2.666E+03
2.999E+03
3.332E+03
3.666E+03
3.999E+03
Orbit file: SENSORFINAL1.TOU
Field file: SENSORFINAL1.EOU
DSnap: 1.00E+00
Plot mode: Standard
Field limits: Autoscale
start
4:25 PM

**(5a)**

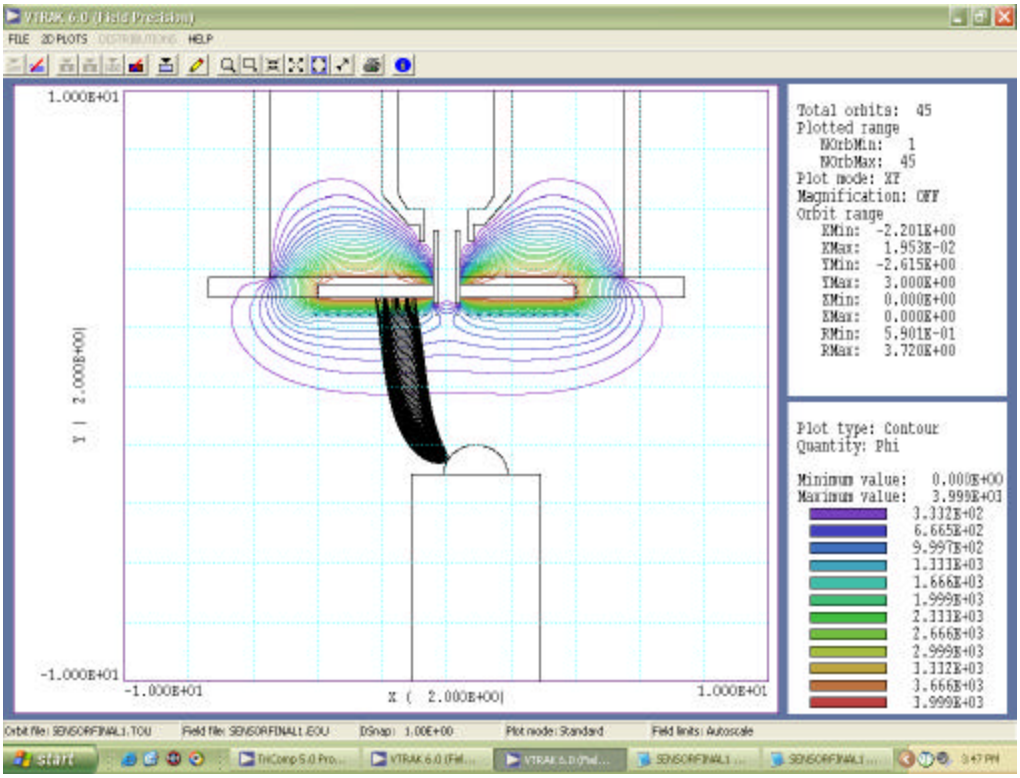
FILE 2D PLOTS HELP
1.000E+01
Y ( 2.000E+00)
-1.000E+01
-1.000E+01
X ( 2.000E+00)
1.000E+01
Total orbits: 45
Plotted range
NOrbMin: 1
NOrbMax: 45
Plot mode: XY
Magnification: OFF
Orbit range
XMin: -2.201E+00
XMax: 1.953E-02
YMin: -2.615E+00
YMax: 3.000E+00
SMin: 0.000E+00
SMax: 0.000E+00
RMin: 5.901E-01
RMax: 3.720E+00
Plot type: Contour
Quantity: Phi
Minimum value: 0.000E+00
Maximum value: 3.999E+03
3.332E+02
6.665E+02
9.997E+02
1.111E+03
1.666E+03
1.999E+03
2.111E+03
2.666E+03
2.999E+03
3.332E+03
3.666E+03
3.999E+03
Orbit file: SENSORFINAL1.TOU
Field file: SENSORFINAL1.EOU
DSnap: 1.00E+00
Plot mode: Standard
Field limits: Autoscale
start
3:47 PM

**(5b)**

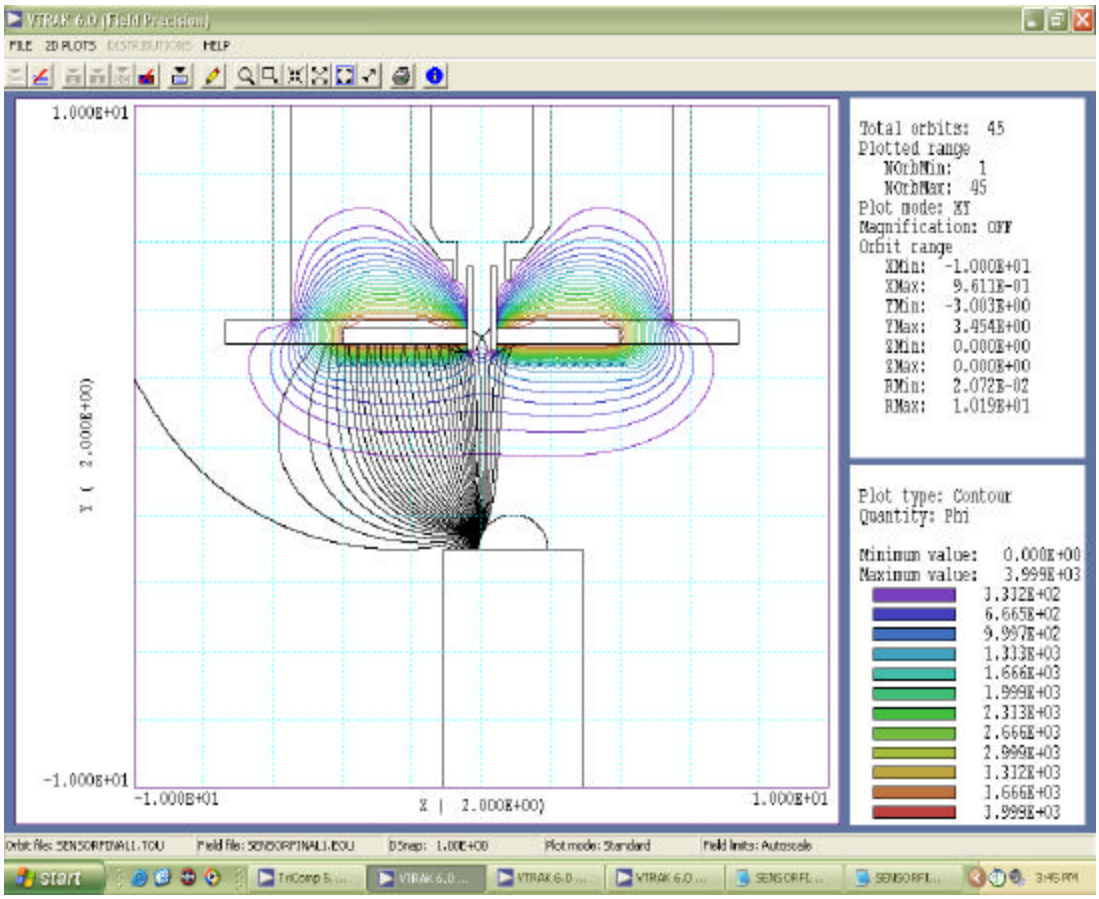


**(5c)**

**Figure 5.** Same design but with piece under test off axis of the electron beam where: (a) shows 50 eV primary particle trajectories, (b) illustrates secondary electron trajectories with 2 eV initial energies, and (c) with 20 eV initial energy trajectories. The primary beam diameter is about an order of magnitude larger than that expected to be generated by the electron gun. A number of different particle trajectories and initial energies were tested in this figure. Table 1 provides some of the design parameters and the initial particle parameters.

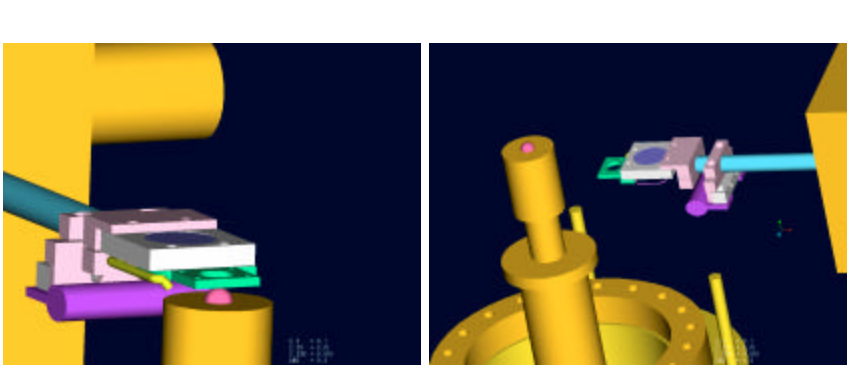


**Figure 6.** Solid model and a line drawing with labels of the XYZ high vacuum manipulator. The manipulator is being used for a number of purposes: target positioning, primary electron beam charge measurements, primary electron beam positioning, *in situ* cleaning of carbon based molecules, and *in situ* cleaning of water molecules.

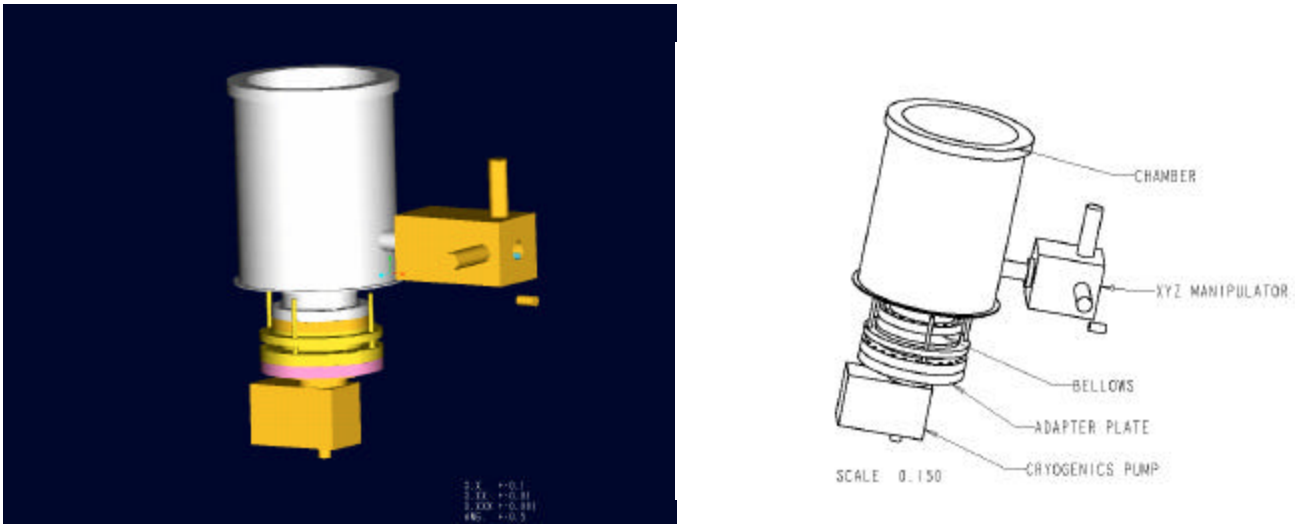


**Figure 7.** Line drawing of the chamber with XYZ manipulator and cryostat with vertical positioning bellows.

3. NO SECTION THREE Purposely left blank so to retain numbering system of figures in section 4.0.

4. Experimental Visualization of the Verification of the Etching Process:

When the CFD results were presented to LANL personnel, they strongly recommended experimental flow visualization of etching process inside the cavity, to help verify FEA simulations and to get better insight into the problem. They also agreed to loan a transparent plastic cavity that will be used at UNLV to simulate etching conditions.

Verification procedure:

a. Compare the CFD results of the LANL baffle under axial exit conditions to the experimental flow under same conditions.
b. The result is then analyzed to verify whether if the CFD and experimental results agree.
c. Design the optimized baffle in such a way so that it could be properly placed inside the cavity.
d. The experiment is repeated using the optimized baffle is then visualized. It is then compared with the CFD results of the optimized baffle.

Experimental setup:
The Setup consists of:

- Arrangement of the cavity and baffle inside the plexiglass box.
- Traversing mechanism for positioning the camera.
- High-speed high resolution CCD camera for capturing images.
- Workstation for controlling the traversing mechanism and the camera.

Vertical configuration:

The initial idea was to have the cavity mounted vertically supported inside the plexiglass tank as shown in the Figure (4.1). This arrangement would however make it difficult to reach the base of tank from inside for connecting the cavity to the exit pipe. The only difference between the horizontal and vertical configurations is the gravity effects. CFD modeling of both configurations indicated that the gravity effect is negligible, which is better explained with the figures shown below.

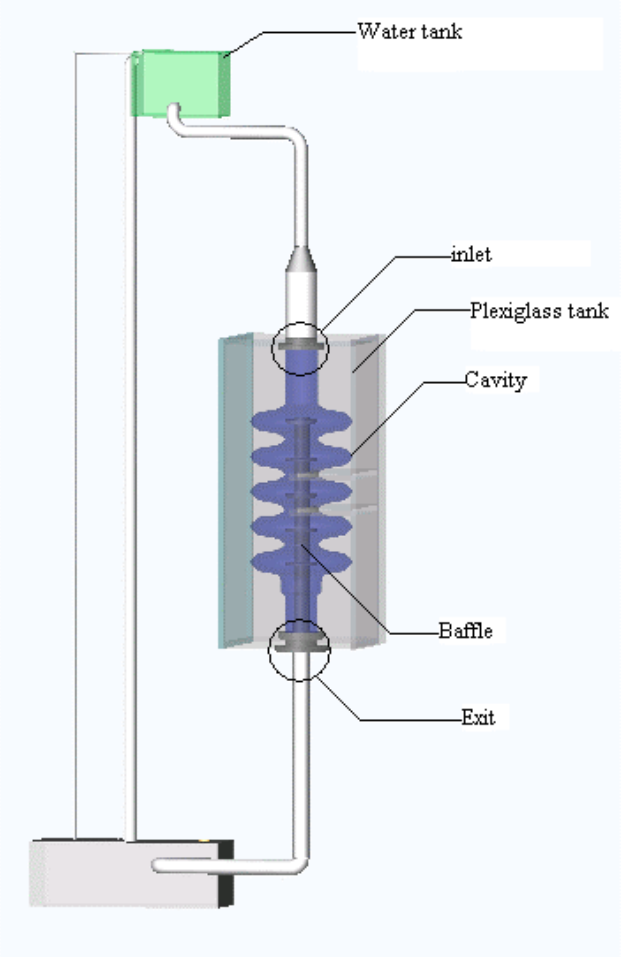


Figure (4.1) Vertical configuration

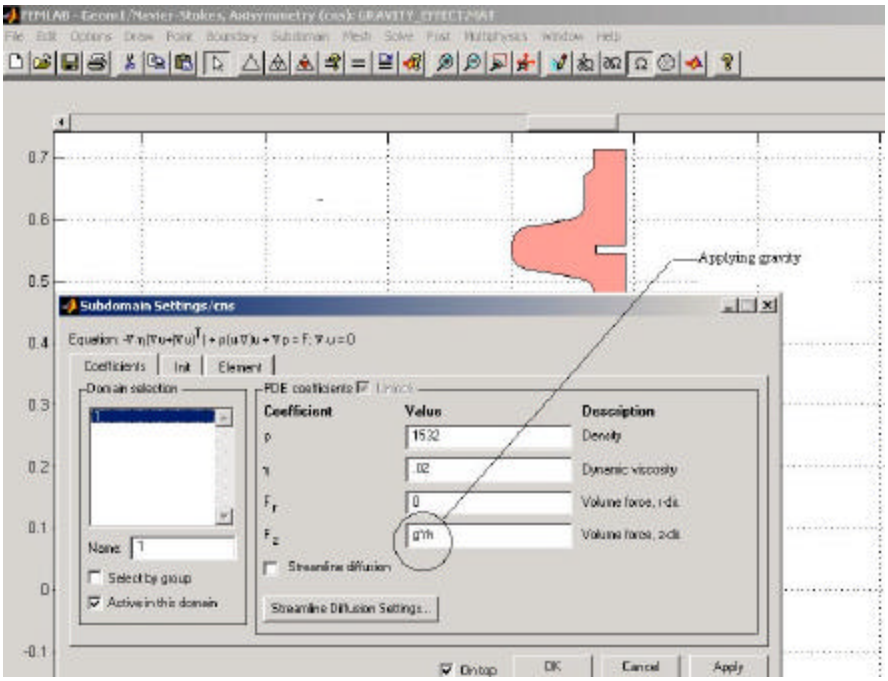


Figure (4.2) CFD model applied with gravity force.

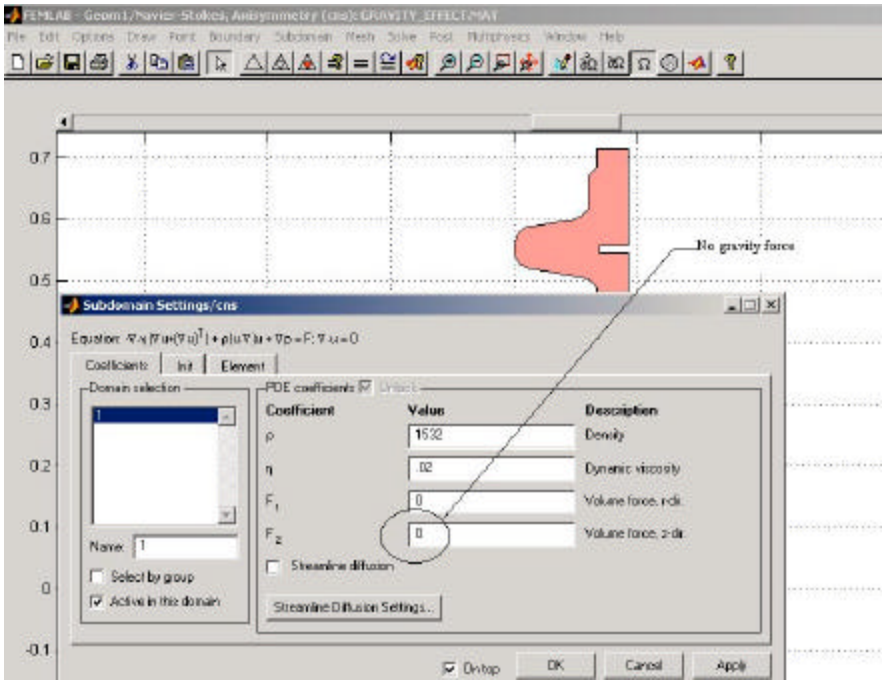


Figure (4.3) CFD model applied without gravity force.

Gravity test results:

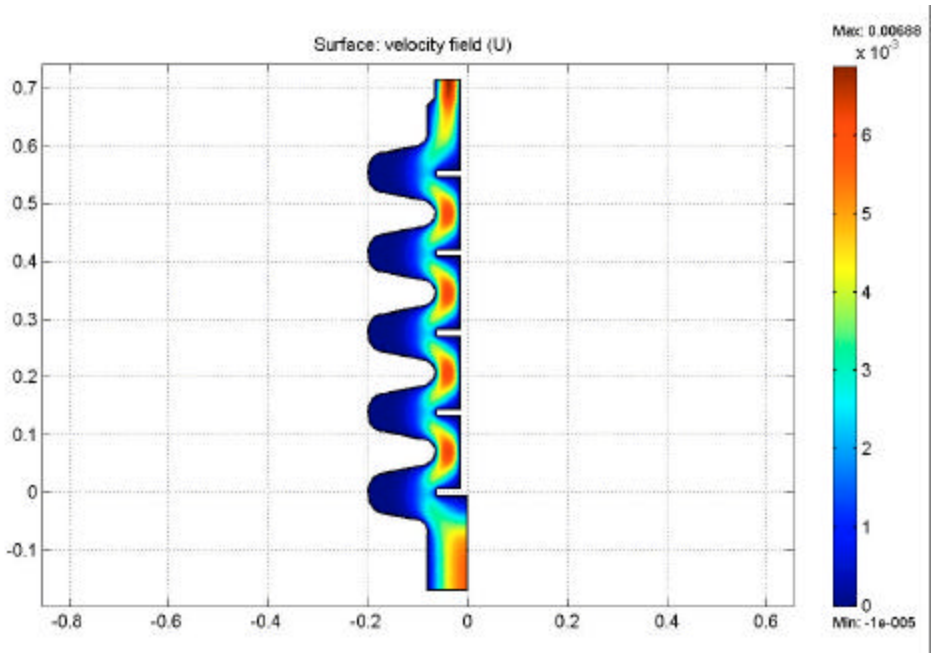


Figure (4.4) Surface plot of CFD model without gravity

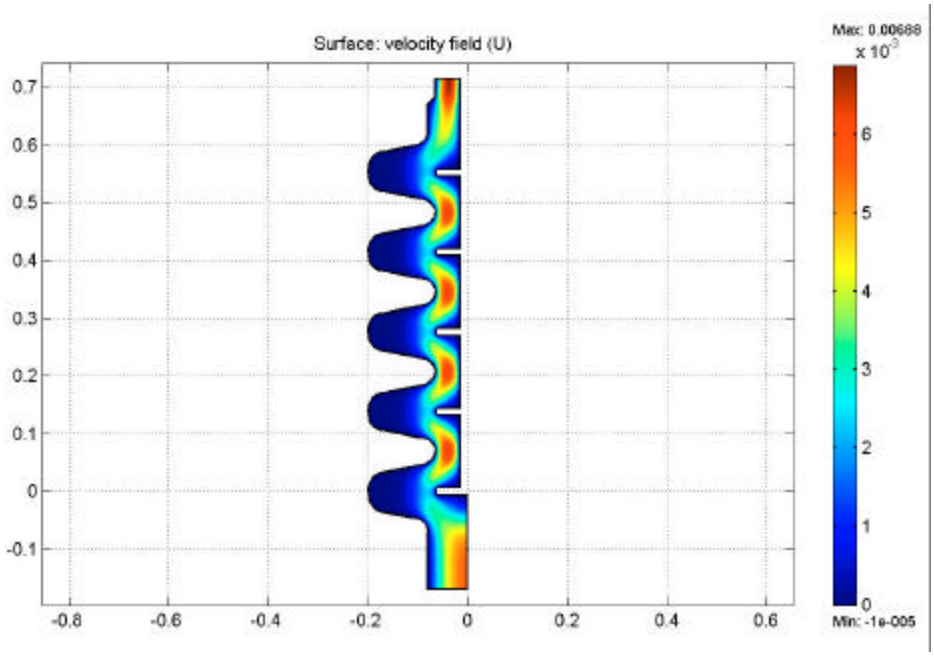


Figure (4.5) Surface plot of CFD model with gravity

From the plots, it is clear gravity is not a significant factor in the flow. In both cases the maximum velocity reached (0.0688 m/s) proved to be the same. So, it is decided to use the

horizontal configuration, Figure (4.6), to better access the cavity. The only problem with the horizontal configuration is the possibility of having a free surface within the cavity during fluid flow. This problem is eventually solved by properly controlling the valves.

Horizontal configuration:

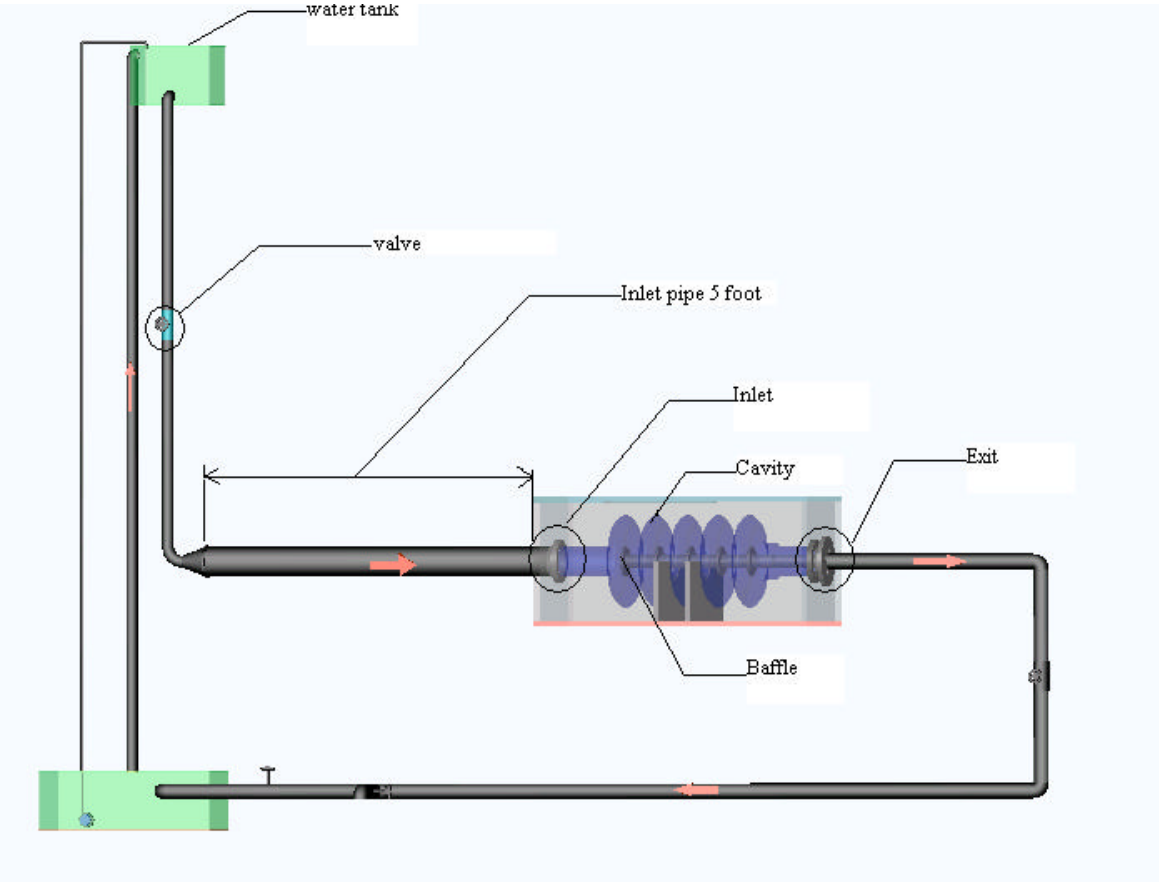


Figure (4.6) Horizontal configuration

In this configuration the cavity is supported by a Plexiglass box, which is filled with water to reduce reflection. The baffle, is placed inside the cavity. Fluid enters the inlet section of the cavity from the tank and exits to reach the bottom tank. Valves are used to control the flow inside the cavity to achieve the required flow rate.

Etching fluid:

Verification of the predicted velocity distributions in a prototype niobium cavity using acid etchant can be hazardous. Fortunately, laminar and turbulent flow distributions can be verified experimentally through dynamic similitude by choosing a fluid flow that has the same Reynolds number for the desired flow rate. Reynolds number is a dimensionless quantity that relates the inertial forces in a fluid to viscous forces. By matching the Reynolds number of the flow in a model to the prototype cavity, the resulting flow patterns will be the same. The velocity of the "model" fluid must be adjusted for differences in fluid density and viscosity. Calculation for velocity for water as model fluid is shown below.

$$\frac{r_e V_e}{m_e} = \frac{r_w V_w}{m_w} \qquad (4.1)$$

The data for the original setup and the experiment are:

| | |
|---|---|
| Density of etching fluid ($?_e$) | 1532 kg/m$^3$ |
| Dynamic viscosity of etching fluid ($\mu_e$) | 0.02 kg/m-s |
| Velocity of etching fluid ($v_{e)}$ | 0.047 m/s |
| Density of water ($?_w$) | 1000 kg/m$^3$ |
| Dynamic viscosity of water ($\mu_w$) | 0.001 kg/m-s |

Table (4.1)

Substituting in equation (4.1), the velocity of water is equal to, 0.0036 m/s in the inlet pipe compared to 0.047m/s (velocity of etching fluid). This corresponds to a flow rate of 43.4 GPH.

**Inlet pipe length:**

For fully developed laminar flow to occur, the length of inlet pipe or the laminar entrance length is given by

$$L_e = 10D \qquad (4.2)$$

Where $L_e$ =laminar entrance length.
D=hydraulic diameter (5 inches)

Which gives $L_e$ =50 inches (4 foot 2 inches) approximated to 5 foot long.

**Traverse mechanism:**

A computer controlled traversing mechanism is used for positioning the camera in the X-Y plane, which is shown below. The controller uses Basic programming language for its operation.

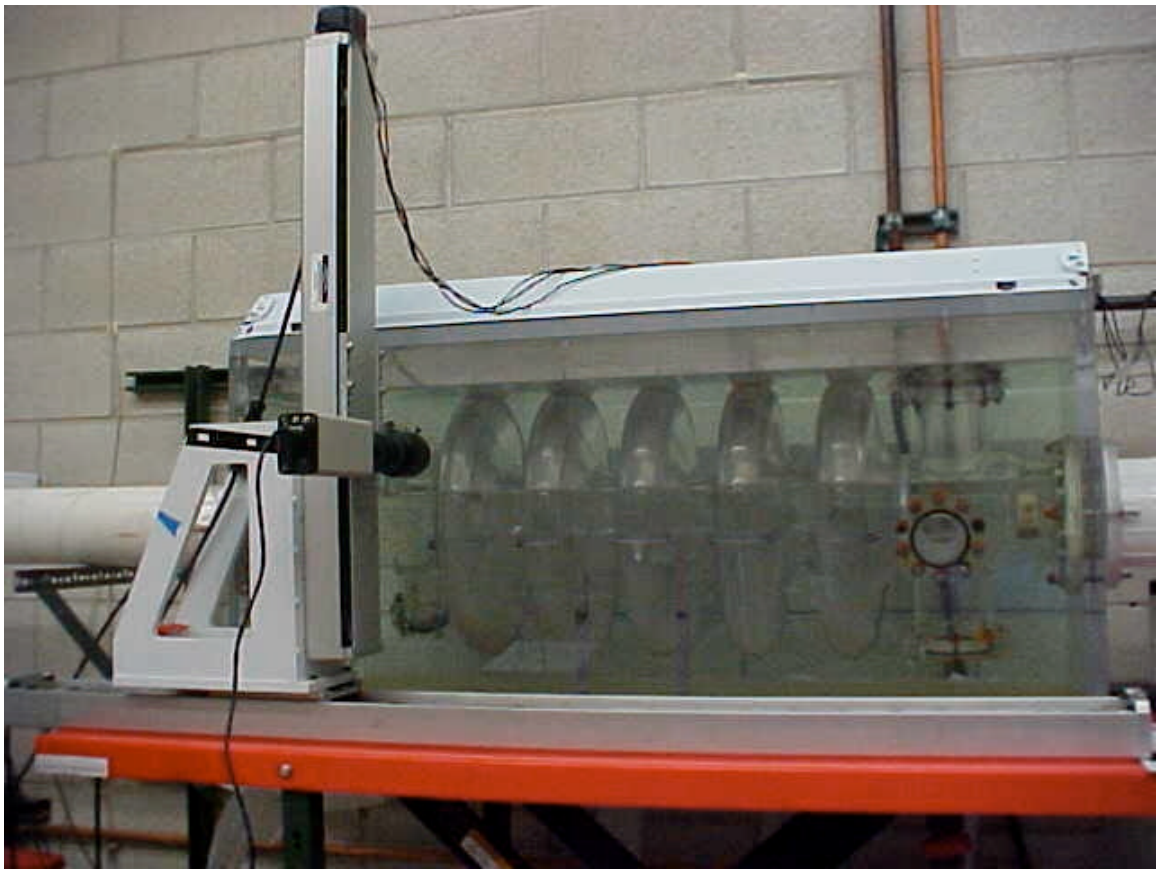

Figure (4.7) Traverse mechanism

The specifications of the controller are:

| | |
|---|---|
| Payload | 5 lb |
| Horizontal Travel (Axis 0) | 48 inches |
| Vertical Travel (Axis 1) | 24 inches |
| Straightness | 0.0005 in/in |
| Positional Accuracy | 0.0005 in/in |
| Drive Type | Screw |
| Motor Type | Stepper |
| Controller | Controller should be able to control two motors with RS-232 ports |

**CCD Camera:**

The flow is photographed using a high-speed high resolution CCD camera.

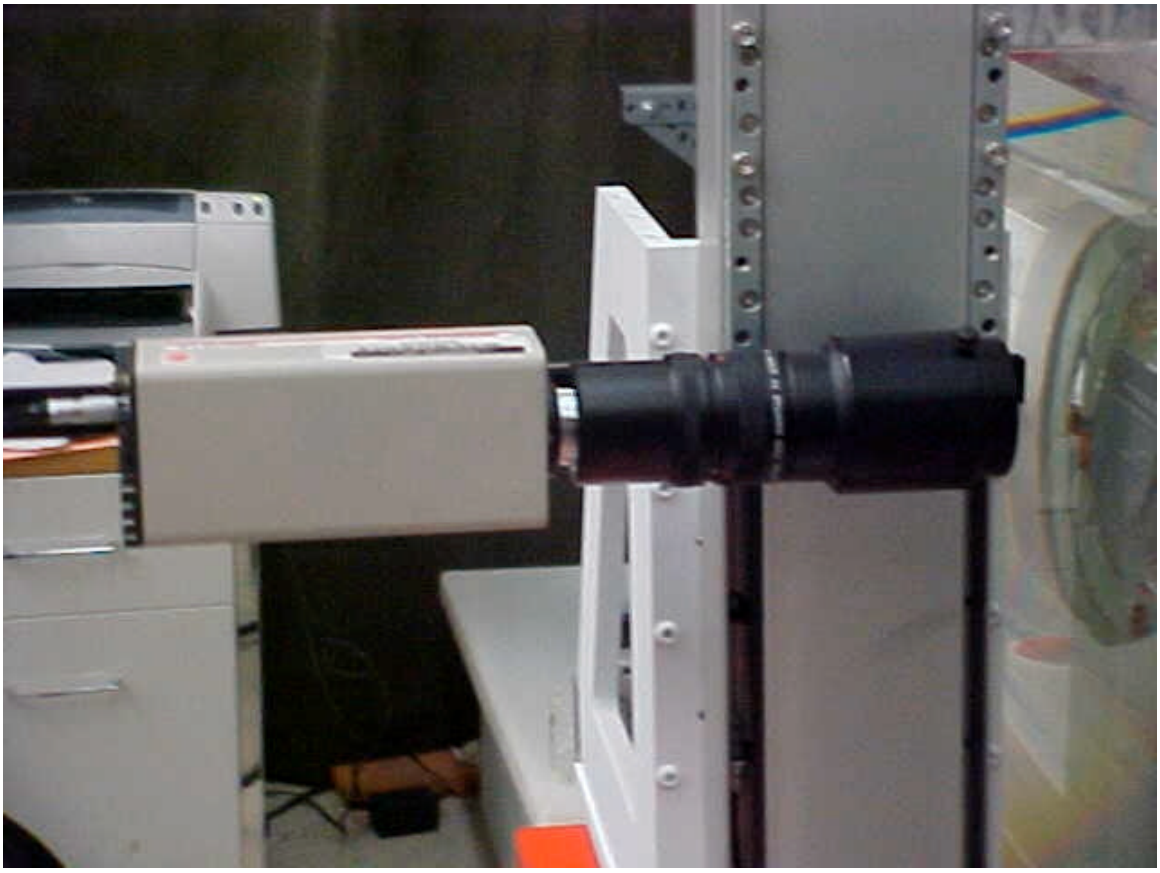

Figure (4.8) CCD camera

The specifications of the camera are given by,

| | |
|---|---|
| Dimensions | 2.0” H ? 2.7” W ? 6.0” L |
| Lens | C-Mount |
| Weight | 1.5 pounds |
| Scanning | Non-interlaced, progressive |
| Synchronization | Pixel clock internal |
| Dynamic Range | 48 db 8-bit, >=58 db 10-bit |
| Pixel clock rate | 20 MHZ |
| Frame rate | 30 fps in dual channel mode<br>15 fps in single channel mode |

**Exit arrangement:**

The CFD results proved that the performance is better when the flow exit is axial to the flow inlet, but it is not practically feasible to create a larger single circular segment for flow exit as it removes the support for the baffle. Instead small circular holes are drilled to achieve the required condition. The effect of replacing the four holes arrangement instead of a single circular segment is also analyzed using the CFD.

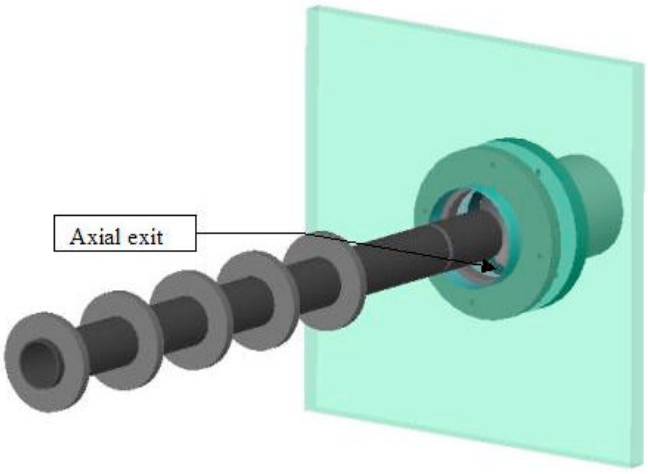


Figure (4.9) Axial exit

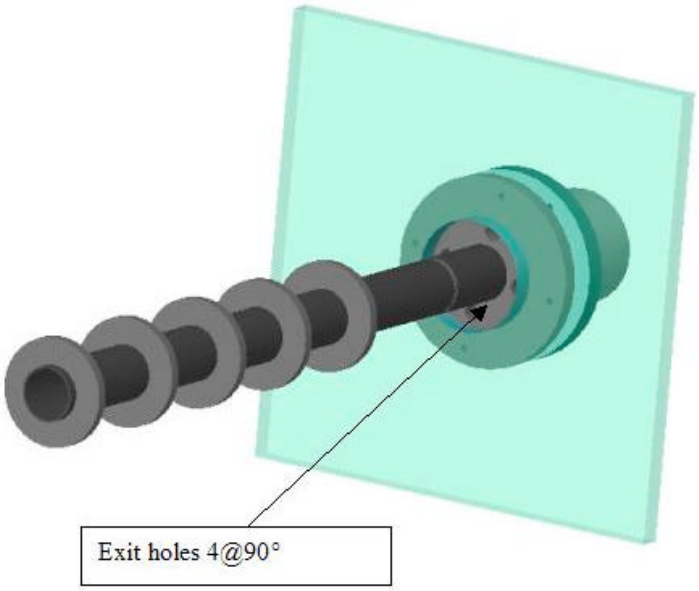


Figure (4.10) Exit through holes

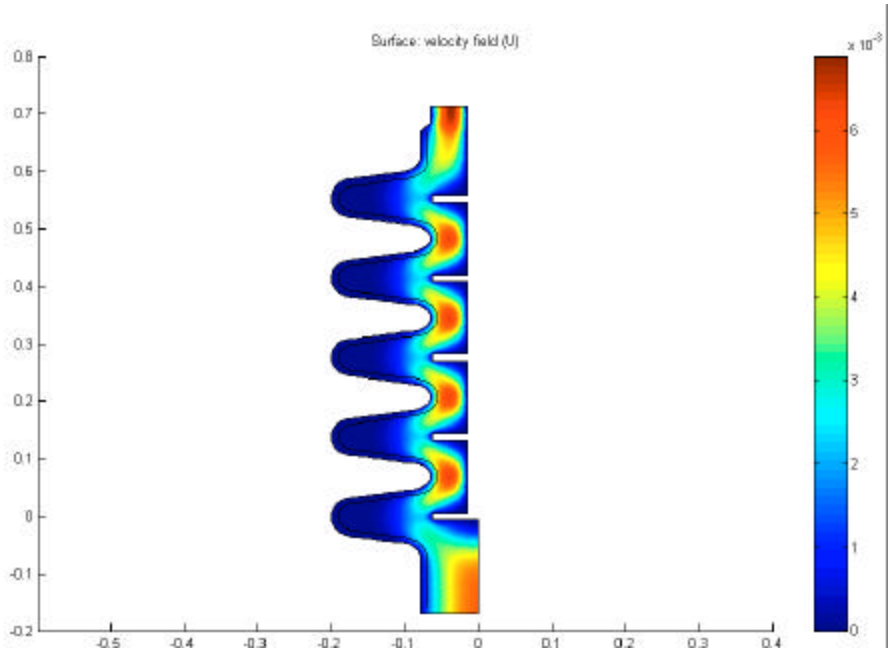


Figure (4.11) CFD plot for axial exit with single circular segment

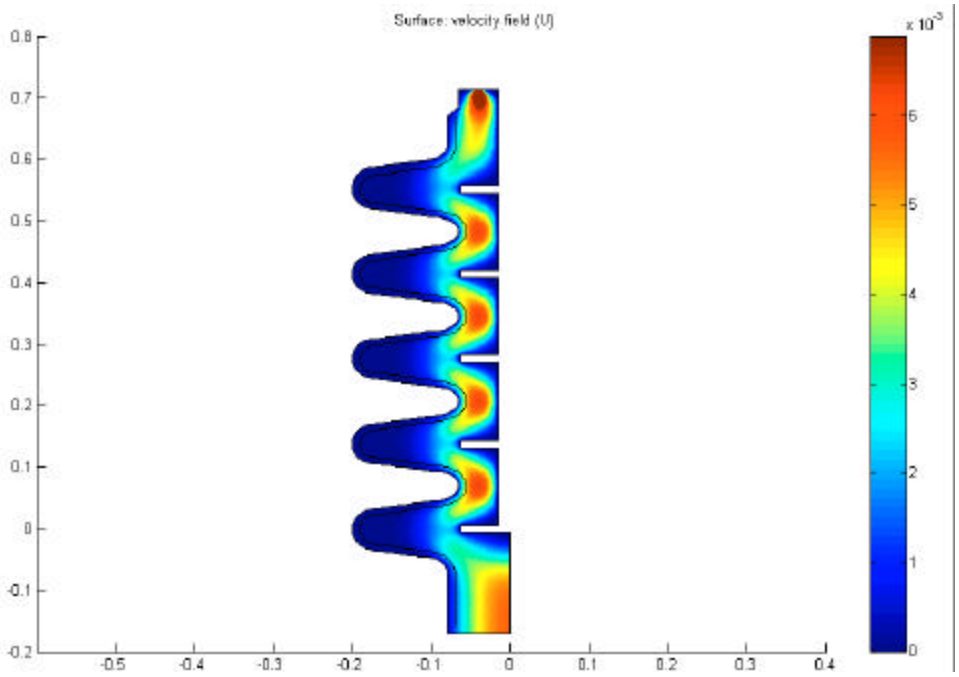


Figure (4.12) CFD plot for axial exit through four holes

Quantitative comparison:

| System | Average velocity | Standard deviation |
|---|---|---|
| Single circular segment | 0.0015154 | 0.23823 |
| Four holes arrangement | 0.0015155 | 0.2382 |

Both the graphical plots and the numerical values prove that four holes arrangement for exit can be substituted for a single circular segment without affecting the results

Experimental procedure:

The pump is switched on, to circulate the water in the system. Valves are properly controlled to make sure the water runs full inside the cavity without any free surface. The discharge is then measured using a measuring jar and a stopwatch. Depending on the discharge obtained the valves are then re-adjusted to maintain the required discharge rate of 0.7238 GPM, once the required discharge rate is obtained, the system is monitored for steady state conditions. If steady state doesn't maintain the process is repeated again until steady flow condition is achieved. The camera is positioned at the required region by the traversing mechanism. The dye is injected Figure (4.13) in the inlet pipe upstream of the inlet section of the cavity and then the flow is photographed with regular time intervals. Using the time difference between the frames and the displacement of the particles the velocity of the fluid is determined. This is better explained with the figures

Figure (4.13) Experimental procedure

The Figure (4.14) shows the position of the dye marked by tiny circles at time 153.781 sec shown in time window. The displacement of the particle in the subsequent frames is shown below.

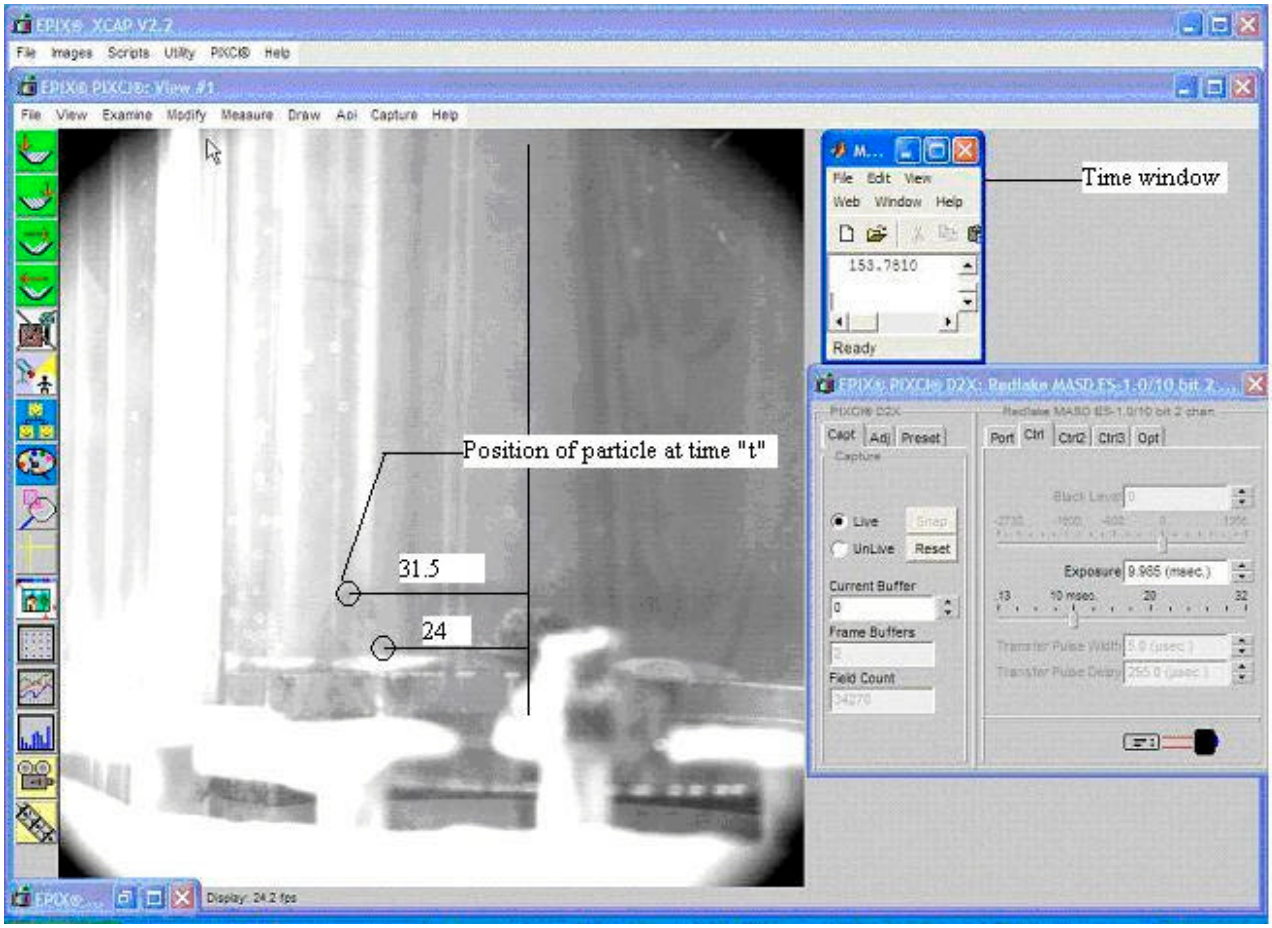


Figure (4.14) Position of dye at time 153.765 sec

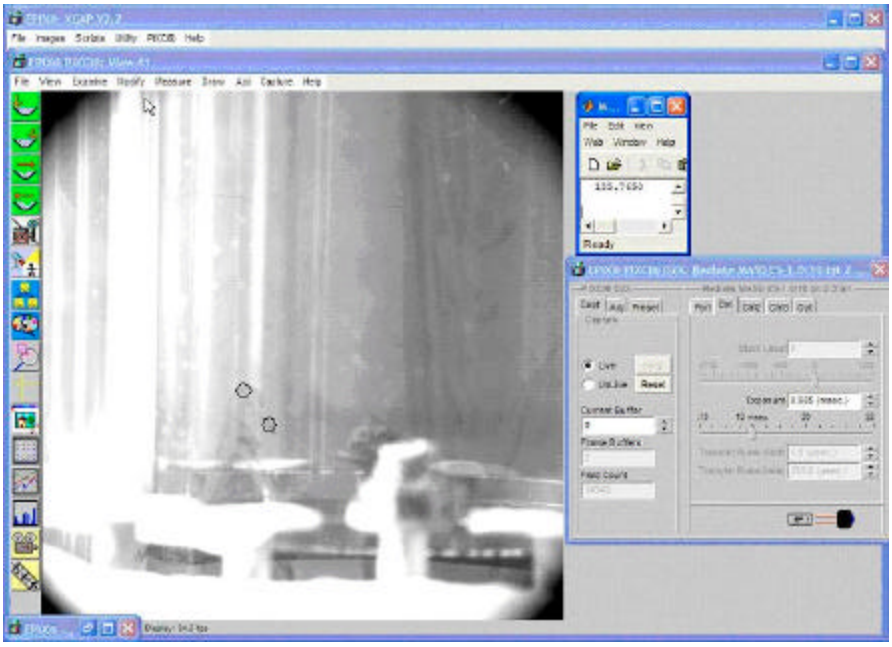

Figure (4.15) Position of dye at time 155.765 sec

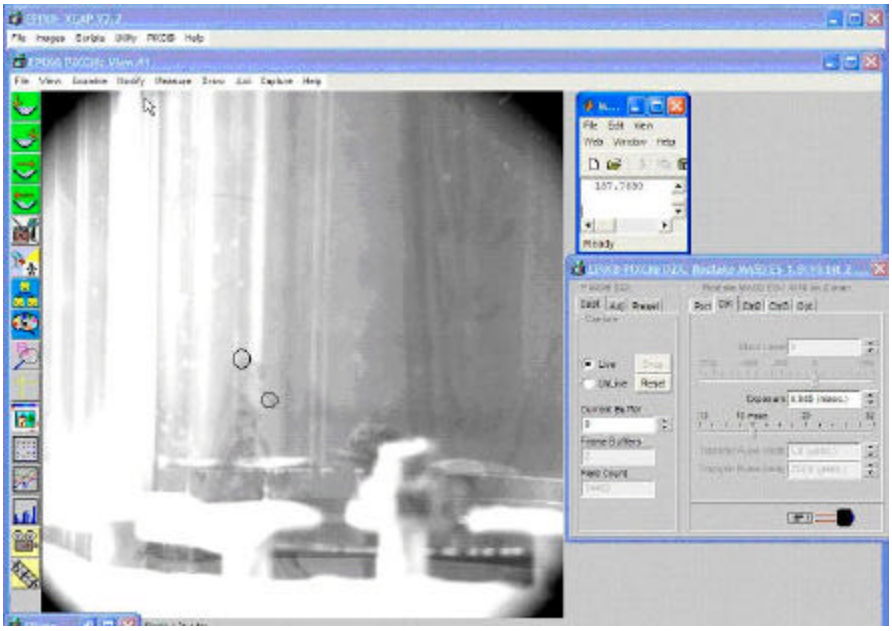

Figure (4.16) Position of dye at time 157.765 sec

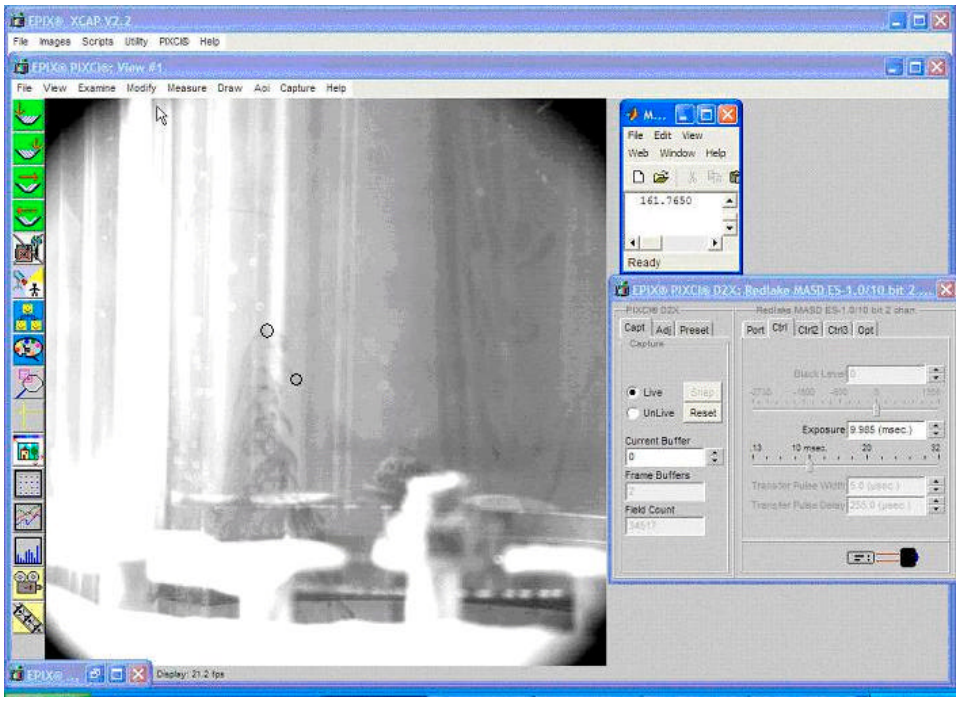

Figure (4.17) Position of dye at time 159.765 sec

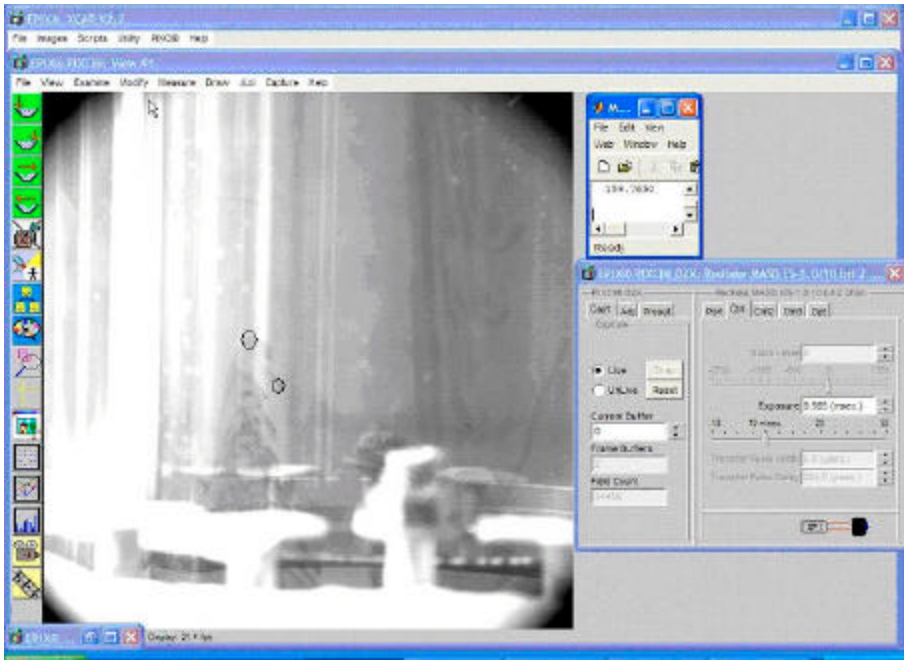

Figure (4.18) Position of dye at time 161.765 sec

In the quantitative calculations a scaling factor of 0.976 has to be considered to convert the displacement in the images to their actual displacement in the real cavity. Accordingly the average velocity at points 30.744mm and 23.248 from the axis of the cavity are calculated by $\frac{\Delta x}{\Delta t}$ is

Table 4.2 velocity values at different time frames

| | Velocity at 30.744 mm from axis mm/s | Velocity at 23.428mm from axis. mm/s |
|---|---|---|
| Frame1-2 | 3.1975 | 2.9516 |
| Frame2-3 | 3.416 | 2.928 |
| Frame3-4 | 2.928 | 2.44 |
| Frame4-5 | 3.416 | 3.172 |
| Average velocity | 3.239 | 2.8729 |

These velocity values are used to interpolate a quadratic function, which is used to approximate the velocity value at any point from the centre line to the end. The section is then divided in to finite annular elements. Each finite area is then multiplied with the corresponding velocity values to get individual discharge for that annular segment, which on summation gives the total discharge, which is equal to 7.63ml/sec. The result is then compared with the discharge measured using measuring jar and stopwatch, which is 9.5ml/sec, close to the experimental result.

LANL Baffle:

Based on the drawings from the LANL the baffle was fabricated using plexiglass Figure (4.19). It is then fixed in to the cavity, which is inside the plexiglass box and analyzed for flow pattern. Figure (4.20) shows the LANL baffle inside the cavity.

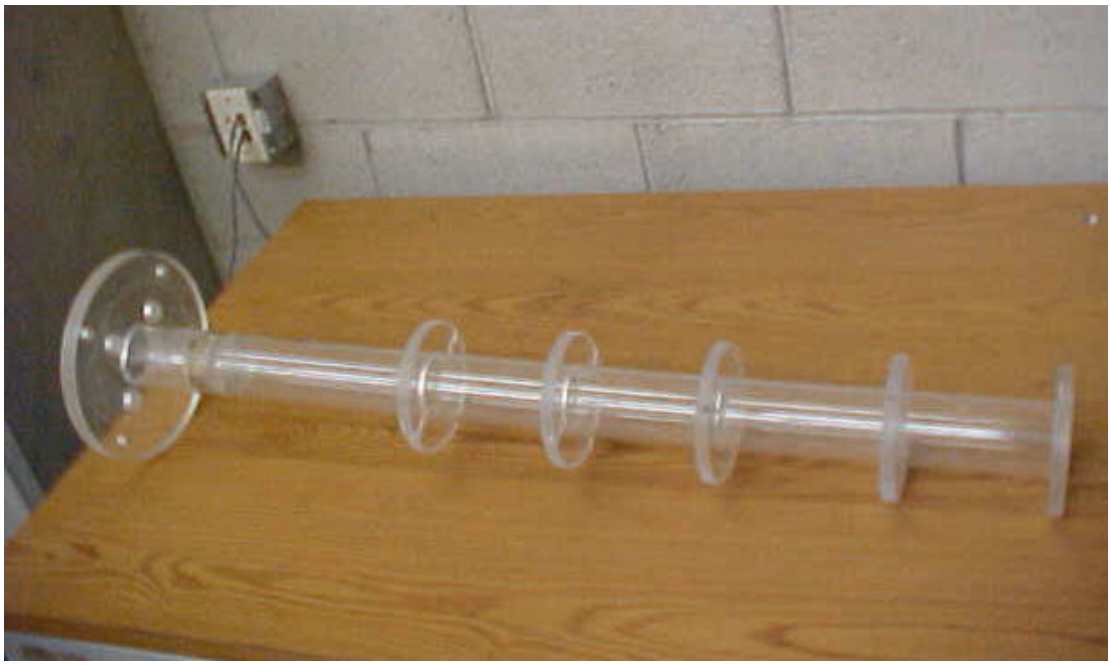

Figure (4.19) Fabricated LANL baffle

LANL Baffle inside cavity:

Figure (4.20) Fabricated LANL baffle inside the cavity

Comparison of CFD versus Experimental results for the LANL baffle:

In the CFD results the streamlines with relatively high velocity values are concentrated in the region 0.08m from the centerline of the cavity, which corresponds to 0.03 from the baffle tip. This high velocity region in the experimental image is identified by band of streamlines, which displace the dye more rapidly, and occurs at a distance of 0.0224 from the baffle tip Figure (4.22). This value is comparable to 0.03m in CFD model. Both results show less penetration inside the cavity cells, with more circulation only near the iris regions

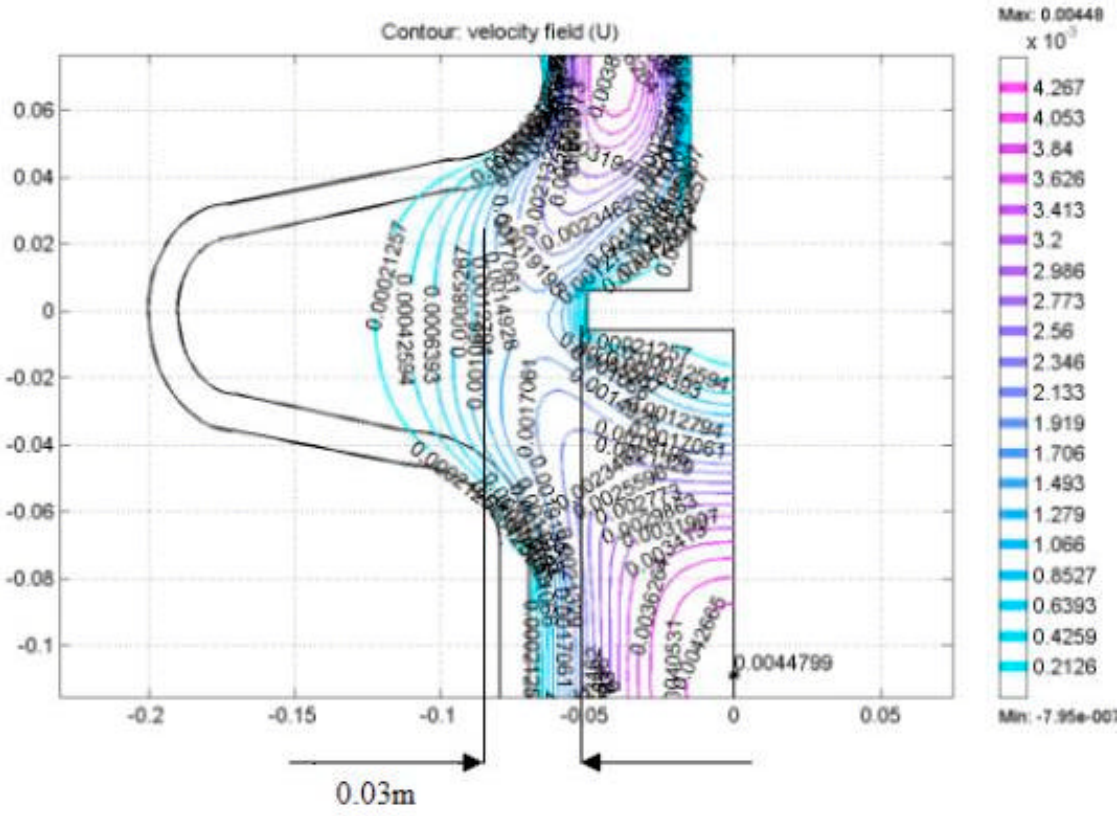


Figure (4.21) CFD velocity plot for LANL baffle

5. Unanticipated Challenges:

- A German company overseas was not aware that money was wired to a bank account for their product. Over a month and a half of time was lost due to this difficulty. In order for the system to work as planned, vendors require information on other vendor's products so that products can be built to fit together as a single unit. Time lost with the German Company has temporarily postponed the building of other associated equipment.

**References**

[1] "A Roadmap for Developing Accelerator Transmuting of Waste (ATW) Technology," DOE/RW-0519, October 1999.

[2] Hasan Padamsee, Jens Knobloch, and Tom Hays, **RF Superconductivity for Accelerators**, Wiley Interscience Publication, John Wiley, N.Y. 1998.

[3] *B. Aune et al., "The Superconducting TESLA Cavities,"* *http://documents.cern.ch/archive/electronic/physics/0003/0003011.pdf*